NEOPLASMA accepted, ahead of print manuscript
Cite article as https://doi.org/10.4149/neo_2025_240925N402

Running title: Necroptosis in prostate cancer

20(S)-ginsenoside Rg3 induced the necroptosis of prostate cancer cells via ROS overproduction

Yanfei Peng[1,2], Yaping Guo[3], Shuwu Zhao[3], Hao Yan[4], Zheng Hao[5], Fang Zheng[3], Zhaiyi Zhang[3], Lin Miao[6], Li-kang Sun[3,*], Muriel Cuendet[2,7,*]

[1]School of Medical Technology, Tianjin University of Traditional Chinese Medicine, Tianjin, China; [2]School of Pharmaceutical Sciences, University of Geneva, Geneva, Switzerland; [3]School of Integrative Medicine, Tianjin University of Traditional Chinese Medicine, Tianjin, China; [4]Department of Oncology, Institute of Integrative Oncology, Tianjin Union Medical Center, Tianjin, China; [5]College of Traditional Chinese Medicine, Tianjin University of Traditional Chinese Medicine, Tianjin, China; [6]State Key Laboratory of Component-based Chinese Medicine, Tianjin University of Traditional Chinese Medicine, Tianjin, China; [7]Institute of Pharmaceutical Sciences of Western Switzerland, University of Geneva, Geneva, Switzerland

*Correspondence: likang.sun@bluewin.ch; muriel.cuendet@unige.ch

Received September 25, 2024 / Accepted March 5, 2025

Necroptosis is a programmed form of necrosis and compounds inducing necroptosis may contribute to cancer treatment. 20(S)-ginsenoside Rg3 is a natural compound extracted from ginseng, which exhibited a broad-spectrum of antitumor activity. In the present study, the potential role of 20(S)-ginsenoside Rg3 in inducing necroptosis in prostate cancer cells was evaluated. 20(S)-ginsenoside Rg3 inhibited the proliferation of prostate cancer cells and upregulated the expression of necroptotic proteins such as receptor-interacting serine/threonine-protein kinase 1 (RIPK1), RIPK3, and their downstream mixed lineage kinase domain-like protein (MLKL). Pretreatment with the selective RIPK1 inhibitor necrostatin-1 (Nec-1) partially reversed the inhibitory effect of 20(S)-ginsenoside Rg3 on prostate cancer cell proliferation. 20(S)-ginsenoside Rg3 led to the accumulation of reactive oxygen species (ROS) and the regulation of autophagy in cancer cells. Scavenging ROS with N-acetyl-L-cysteine (NAC) antagonized the regulatory effects of 20(S)-ginsenoside Rg3 on cell autophagy and necroptotic proteins expression. Moreover, 20(S)-ginsenoside Rg3 exhibited an antitumor effect in a prostate cancer xenograft mouse model in which it upregulated the expression of RIPK1, RIPK3, MLKL and led to a decrease in tumor weight, as well as an increase in necrotic areas in tumor tissue. In conclusion, our study showed that 20(S)-ginsenoside Rg3 might induce necroptosis in prostate cancer *in vitro* and *in vivo* via the ROS/autophagy signaling pathway.

Key words: autophagy; 20(S)-ginsenoside Rg3; necroptosis; prostate cancer; reactive oxygen species

Prostate cancer remains an important health issue since it was the second most frequent cancer and the fifth leading cause of cancer death among men worldwide in 2022 [1]. Prostate cancer is initially sensitive to anti-androgen therapy. However, during the course of the treatment, prostate cancer often becomes refractory to hormone therapy and develops into castration-resistant prostate

cancer (CRPC), which is also resistant to chemotherapy [2]. Therefore, there is no satisfactory treatment against CRPC and it is urgent to develop new therapeutic options.

Necroptosis is a form of programmed cell death that resembles necrosis and depends on a unique molecular pathway different from apoptosis. The formation of a RIPK1-RIPK3 necrosome through auto- and trans-phosphorylation of RIPK1 and RIPK3 happens at the initiation of necroptosis [3]. This is followed by MLKL activation via phosphorylation and translocation to the plasma membrane which causes cell death. Given the resistance of cancer cells to apoptosis, the induction of necroptosis may be an alternative strategy for cancer therapy [4, 5]. Previous studies indicated that RIPK3 expression was often silenced in cancer cells due to genomic methylation near the transcriptional start site of *RIPK3*. This repressed necroptosis-induced cell death suggests that inducing necroptosis may be beneficial for cancer treatment [6]. In prostate cancer tissues, the expression of RIPK3 was elevated at early stages of cancer, while it was repressed at late stages, and negatively correlated with tumor size and prostate-specific antigen (PSA) levels [7]. Another study reported the down-regulation of RIPK3 in prostate cancer cell lines and clinical prostate tumor samples. Low expression of RIPK3 was closely related to tumor metastasis and poorer survival, while up-regulation of RIPK3 could induce necroptosis and alleviate prostate cancer progression [8]. Moreover, sirtuin 3 (SIRT3) and SIRT6 were increased in prostate cancer tissues and this induced prostate cancer progression by inhibiting RIPK3-mediated necroptosis and innate immune response [9]. Several natural compounds have been reported to induce necroptosis and may be beneficial in the treatment of prostate cancer. Ophiopogonin D, a compound extracted from *Ophiopogon japonicus*, exhibited an antiproliferative activity in androgen-dependent prostate cancer cells via the induction of a RIPK1- and MLKL-dependent necroptosis [10]. Arctigenin, a natural product isolated from *Arctium lappa*, also induced necroptosis in acidity-tolerant prostate cancer cells via ROS-mediated mitochondrial damage and the upregulation of cell communication network factor 1 (CCN1) [11]. Hong et al reported that the rosin derivative IDOAMP increased the phosphorylation of RIPK1, RIPK3, MLKL and activated necroptosis in prostate cancer cells [12]. Moreover, a recent report indicated that emodin induced necroptosis in prostate cancer cells via the regulation of the mitochondrial fission pathway [13]. These studies highlight a potential strategy for prostate cancer treatment via agent-induced necroptosis.

20(S)-ginsenoside Rg3 is clinically used against several cancers and displays a remarkable antitumor activity via multiple mechanisms [14, 15]. Several studies reported that 20(S)-ginsenoside Rg3 inhibited the proliferation and migration of prostate cancer cells as well as enhanced the susceptibility of prostate cancer cells to docetaxel [16-18]. Our previous work indicated that 20(S)-ginsenoside Rg3 upregulated ROS levels and induced cell cycle arrest to inhibit

the proliferation of PC3, a human CRPC cell line [19]. The regulatory role of 20(S)-ginsenoside Rg3 was also reported in the prostatic microenvironment with an inhibition of senescence in prostate stromal cells through down-regulation of interleukin 8 (IL-8) expression [20]. In this study, we explored the *in vitro* and *in vivo* potential effects and underlying mechanisms of 20(S)-ginsenoside Rg3 on the regulation of necroptosis in prostate cancer cells.

Materials and methods

Cell lines and reagents. The prostate cancer cell lines 22RV1 and PC3 were purchased from American type culture collection (ATCC, Manassas, VA, USA) and cultured in RPMI1640 medium (Sigma, St Louis, MO, USA) supplemented with 10% fetal bovine serum (FBS, Lonsera Science SRL, Canelones, Uruguay). 20(S)-ginsenoside Rg3 (CAS: 14197-60-5) was purchased from Weikeqi Biological Technology Col, Ltd (Chengdu, Sichuan, China) and dissolved in dimethyl sulfoxide (DMSO, purchased from Solarbio, Beijing, China). N-acetyl-L-cysteine (NAC) was purchased from Beyotime institute of biotechnology (Shanghai, China), and Nec-1 from Med Chem Express (Monmouth Junction, NJ, USA).

Analysis of online databases. The Genotype-Tissue Expression (GTEx) and The Cancer Genome Atlas (TCGA) databases were analyzed with an online tool (www.xiantaozi.com) to compare the expression of *RIPK1*, *RIPK3* and *MLKL* in normal prostate and prostate tumor samples (100 normal tissues, 496 tumor tissues and 52 para-cancerous tissues). Wilcoxon rank sum test and paired sample *t*-test were applied for statistical analysis. Disease specific survival analysis and receiver operating characteristic curve (ROC) analysis were also operated with the same tool. The diagnostic efficiencies of *RIPK1*, *RIPK3* and *RIPK3* in prostate tumor was compared with DeLong's test.

CCK8 assays. 22RV1 and PC3 cells were seeded into 24-well plates (1×10^4 cells/well) and treated with vehicle (DMSO, final concentration 0.1%), 50 or 100 μM 20(S)-ginsenoside Rg3 for 0, 24, 48 or 72 h. Then, a CCK8 kit (US Everbright INC, Suzhou, China) was used to evaluate the proliferation of cells according to the manufacturer instructions. The results are expressed as the mean±SD of three independent experiments.

Flow cytometry assays. 22RV1 and PC3 cells were cultured into 6-well plate (1×10^5 cells/well) and treated with DMSO (final concentration 0.1%) or 100 μM 20(S)-ginsenoside Rg3 for 48 h. Cells were digested with 0.25% trypsin (Solarbio) to detach from the plate and then a FITC-Annexin V and PI apoptosis kit (US Everbright) was used to label suspended cells according to the manufacturer instructions. Cell apoptosis and necrosis were analyzed by flow cytometry (Guava easyCyte b-2L, Millipore, Billerica, MT, USA). The proportion of cell subtypes are expressed as the mean±SD of three independent experiments. To evaluate the ROS level, 22RV1 and PC3 cells

118 were cultured into 6-well plates (1×10^5 cells/well) and treated with DMSO (final concentration
119 0.1%) or 100 μM 20(S)-ginsenoside Rg3 for 48 h, and subsequently labeled with 2,7-
120 dichlorodihydrofluorescein diacetate (DCFH-DA, Beyotime). Then flow cytometry assays were
121 performed to evaluate the ROS levels in cells and the assays were performed three times
122 independently.
123 **Western blot analysis.** 22RV1 and PC3 cells were cultured into 6-well plate (1×10^5 cells/well)
124 and then treated with DMSO (final concentration 0.1%) or 100 μM 20(S)-ginsenoside Rg3 for 48 h.
125 Total proteins were extracted with radio immunoprecipitation assay (RIPA) buffer (CWBIO,
126 Beijing, China) supplemented with 1 mM phenylmethanesulfonylfluoride (PMSF, Solarbio). The
127 protein concentration was quantified using the BCA method (CWBIO). Then, western blot analysis
128 was performed using the following antibodies (Cell Signaling Technology, Danvers, MT, USA):
129 RIPK1 (#3493, dilution 1:1000), RIPK3 (#13526, dilution 1:1000), MLKL (#14993, dilution
130 1:1000) and the HRP-linked second antibody (anti-rabbit, #7074, dilution 1:2500). LC3 (#bs-8878R,
131 dilution 1:1000) and p62 antibodies (#bs-55207R, dilution 1:1000) were purchased from Bioss
132 (Beijing, China). Caspase 3 antibody (#ab13847, diluted at 1:1000) was purchased from Abcam
133 (Cambridge, UK). Protein expression was normalized to glyceraldehyde-3-phosphate
134 dehydrogenase (GAPDH, #AB0037, Abways, dilution 1:12000). All the experiments were
135 performed three times independently. Quantitative analyses of the results were performed using
136 Image J software.
137 **Nec-1 and NAC pretreatment.** 22RV1 and PC3 cells were cultured into 6-well plates (1×10^5
138 cells/well) and then pretreated with 10 mM NAC for 1 h, followed by a treatment with DMSO (final
139 concentration 0.1%) or 100 μM 20(S)-ginsenoside Rg3 for 48 h to extract total proteins for western
140 blot analyses. 22RV1 and PC3 cells were also cultured into 24-well plate (1×10^4 cells/well) and
141 pretreated with 100 μM Nec-1 for 1 h, followed by a treatment with DMSO (final concentration
142 0.1%) or 100 μM 20(S)-ginsenoside Rg3 for 72 h to measure cell proliferation using a CCK8 kit.
143 The experiments were performed independently for three times and the results of CCK8 assays are
144 expressed as the mean±SD.
145 **Mice xenograft model.** The protocol for *in vivo* studies was approved by the Experimental Animal
146 Ethics Committee of the Institute of Radiation Medicine, Chinese Academy of Medical Sciences
147 (Approval No. IRM-DWLL-2019157). Sixteen Balb/c nude mice (male, 6 weeks old) were
148 purchased from Huafukang Biotechnology Company (Beijing, China). The mice were acclimated in
149 specific pathogen-free units for 1 week, followed by subcutaneous injection of 5×10^6 PC3 cells on
150 the right side of the armpit. Mice were normally fed for another 2 weeks and divided into two
151 groups: control group (eight mice) and ginsenoside Rg3 treatment group (eight mice). Daily gavage

with phosphate buffer saline (PBS) was performed in the control group and daily intragastric gavage with 20(S)-ginsenoside Rg3 (25 mg/kg body weight) was performed in the treatment group for 2 weeks. Body weight and tumor volumes were monitored every two days. The volume of tumors was calculated with the formula: $V=1/2 \times \text{long diameter} \times (\text{short diameter})^2$. At the end of the treatment, mice were sacrificed and the xenografts were collected for hematoxylin-eosin (H&E) staining, immunofluorescent (IF) staining and western blot analysis.

H&E and IF staining. Each tissue sample was separated in two parts. One part was embedded in paraffin and the other one was frozen. The paraffin sections were used to perform H&E staining and the pictures were taken using an optical microscope (Leica, Wetzlar, Germany) at 100, 200 and 400× magnification. The frozen sections were blocked in PBS supplemented with 10% FBS. RIPK1 (bs-5805R, dilution 1:200), RIPK3 (bs-3551R, dilution 1:200) and MLKL (bsm-33339M, dilution 1:200) antibodies were purchased from Bioss and the secondary antibodies (CoraLite594-conjugated recombinant rabbit anti-mouse IgG and CoraLite488-conjugated goat anti-rabbit IgG) were both purchased from Proteintech. 4',6-Diamidino-2-phenylindole (DAPI, Solarbio) was used to label the nucleus. Pictures were taken with a fluorescence microscope (Leica DMi8) at 200× magnification.

Statistical analysis. All statistical analyses were performed using SPSS software (version 23.0; IBM Corp., Armonk, USA). Data are presented as the mean±SD. *t*-Tests were used to analyze the data between two groups. One-way ANOVA and Turkey's post hoc correction was performed when there were multiple groups. $P < 0.05$ indicates statistical significance.

Results

The expression of necroptotic genes was down-regulated in prostate cancer compared to normal prostate samples. Necroptosis may contribute to prevent the progression of carcinogenesis since the expression of its key mediator RIPK3 is decreased in several types of cancer cells. To validate the potential effect of necroptosis in prostate cancer, the expression of *RIPK1*, *RIPK3* and *MLKL* was explored in normal prostate and cancer tissues with data obtained through the GTEx and TCGA databases. A higher expression of *RIPK1* was observed in normal tissues compared to prostate cancer tissues. Moreover, the expression of *RIPK3* and *MLKL* was also down-regulated in prostate cancer samples compared to either normal tissues or corresponding para-cancerous tissues (Figures 1A, 1B). In consideration of these results, the diagnostic potential of *RIPK1*, *RIPK3* and *MLKL* for prostate cancer was compared using a ROC analysis and results indicated that *RIPK3* (AUC=0.903) had a higher diagnostic efficiency for prostate cancer compared to *RIPK1*

185 (AUC=0.685) and *MLKL* (AUC=0.854) (Figure 1C). Furthermore, survival analysis was performed
186 and lower expression of *RIPK3* was correlated with poor disease specific survival (Figure 1D).
187 **20(S)-ginsenoside Rg3 induced the expression of necroptotic genes in prostate cancer cells.**
188 Our previous research indicated that 20(S)-ginsenoside Rg3 induced cell cycle arrest in PC3 cells
189 [19]. In the present study, the inhibitory effects of 20(S)-ginsenoside Rg3 on cell proliferation were
190 observed both in 22RV1 and PC3 cells. The cells were treated with various doses of 20(S)-
191 ginsenoside Rg3 (0, 50 and 100 μM) for 24, 48 and 72 h. CCK8 assays confirmed that 50 and 100
192 μM 20(S)-ginsenoside Rg3 inhibited the proliferation of 22RV1 cells at all three time points (Figure
193 2A). In PC3 cells, 100 μM 20(S)-ginsenoside Rg3 inhibited cell proliferation at 24, 48 and 72 h,
194 while 50 μM 20(S)-ginsenoside Rg3 did not exhibit the inhibitory effects on cell proliferation at 72
195 h (Figure 2B). The percentage of apoptotic and necrotic cells in 22RV1 and PC3 cells treated with
196 100 μM 20(S)-ginsenoside Rg3 for 48 h was also evaluated by flow cytometry with a FITC-
197 Annexin V and PI apoptosis assay (Figure 2C). 20(S)-ginsenoside Rg3 increased the proportion of
198 late apoptotic/necrotic ($PI^+/FITC^+$) cells and decreased the proportion of viable cells ($PI^-/FITC^-$) in
199 both 22RV1 and PC3 cells (Figures 2D, 2E). Treatment with 100 μM 20(S)-ginsenoside Rg3 for 48
200 h did not regulate the expression and cleavage of caspase 3 both in 22RV1 and PC3 cells,
201 suggesting that 20(S)-ginsenoside Rg3 may induce necroptosis rather than apoptosis in prostate
202 cancer cells (Figure 2F). To explore the potential regulatory effects of 20(S)-ginsenoside Rg3 on
203 cell necroptosis, western blots were performed and the results showed that treatment with 100 μM
204 20(S)-ginsenoside Rg3 for 48 h led to an increase in the expression of RIPK1, RIPK3 and MLKL,
205 suggesting that 20(S)-ginsenoside Rg3 might induce necroptosis in prostate cancer cells (Figures
206 3A, 3B). Pretreatment with the 100 μM RIPK1 inhibitor Nec-1 for 1 h at least partially reversed the
207 inhibitory role of 20(S)-ginsenoside Rg3 on the proliferation of prostate cancer cells (Figure 3C).
208 **20(S)-ginsenoside Rg3 blocked the autophagy flux and up-regulated the expression of**
209 **necroptotic proteins in prostate cancer cells via ROS accumulation.** ROS plays an important
210 role in the modulation of cell fate. Our previous report indicated that 20(S)-ginsenoside Rg3
211 elevated ROS level in PC3 cells in a dose-dependent manner [19]. In the present study, the
212 accumulation of ROS was observed both in 22RV1 cells and PC3 cells in the treatment with 100
213 μM 20(S)-ginsenoside Rg3 for 48 h using the DCFH-DA dye followed by flow cytometry analysis
214 (Figure 4A). Since there is a crosstalk between cell autophagy and necroptosis, the regulatory effect
215 of 20(S)-ginsenoside Rg3 on cell autophagy was also explored. The lipidation of LC3 and the
216 protein expression of p62 were both increased by 20(S)-ginsenoside Rg3 (100 μM for 48 h) in
217 22RV1 and PC3 cells, suggesting that 20(S)-ginsenoside Rg3 inhibited the late autophagy and
218 decreased the autophagy flux in prostate cancer cells (Figures 4B, 4C). NAC, a ROS scavenger,

reversed the regulatory role of 20(S)-ginsenoside Rg3 in LC3 lipidation and p62 protein expression, indicating that 20(S)-ginsenoside Rg3 blocked the autophagy flux via the accumulation of cellular ROS (Figures 4D, 4E). Moreover, pretreatment with 10 mM NAC for 1 h also blocked the up-regulation of RIPK1, RIPK3 and MLKL protein expression in 22RV1 and PC3 cells induced by 100 μM 20(S)-ginsenoside Rg3, suggesting that the compound might increase necroptosis via the accumulation of ROS and subsequent blockage of autophagy flux (Figures 4F, 4G).

20(S)-ginsenoside Rg3 up-regulated the expression of necroptotic proteins in PC3 mice xenografts. To evaluate the *in vivo* effect of 20(S)-ginsenoside Rg3, a PC3 mouse xenograft model was established by subcutaneous injection of PC3 cells in the right side of the armpit. Two weeks later, daily gavage with PBS or 20(S)-ginsenoside Rg3 (25 mg per kg body weight) was performed for additional 2 weeks. Then, the mice were sacrificed, and the volume and weight of the tumors were measured. No obvious differences were observed for the volume of tumors between the control and 20(S)-ginsenoside Rg3-treated groups though tumors in the latter looked smaller (Figures 5A, 5B). However, the weights of tumors decreased after 20(S)-ginsenoside Rg3 treatment (Figure 5C). HE staining was performed to detect the histological features of the tumors and the results showed that 20(S)-ginsenoside Rg3 increased a necrosis-like phenotype in the tissues with more ruptured nuclei and disintegrated cells (Figure 5D). IF staining was also performed and the results showed that 20(S)-ginsenoside Rg3 led to an upregulation of the expression of RIPK1, RIPK3 and MLKL in tumor tissues (Figure 5E). Finally, protein expression of RIPK1, RIPK3 and MLKL was upregulated in xenografts isolated from the 20(S)-ginsenoside Rg3-treated group compared to the control (Figures 5F, 5G).

Discussion

Necroptosis is recognized as a programmed necrotic cell death and is triggered by several intrinsic factors, such as tumor necrosis factor (TNF) and interferon (IFN) [21]. Although the formation of the necrosome, which is composed of RIPK1 and RIPK3 has been considered as a feature of necroptosis, the actual mechanism is much more complicated. In addition to forming the necrosome, RIPK1 can also mediate RIPK1-dependent apoptosis and the decision to which way the cells die may be determined by mitogen-activated protein kinase 7 (MAP3K7, also known as TAK1) [22]. RIPK3 was reported to mediate RIPK1-independent necroptosis via its interaction with TNFRSF1A associated via death domain (TRADD) to activate the RIPK3-MLKL signaling pathway [23]. Recent research disclosed a new regulatory mechanism of necroptosis in which linear ubiquitin chain assembly complex (LUBAC) was identified as a novel checkpoint for necroptosis. LUBAC and it mediated M1 poly-ubiquitination modification promoted MLKL membrane accumulation and

253 subsequent cell necroptosis in human cells without affecting the phosphorylation of RIPK1, RIPK3
254 and MLKL or necrosome formation [24]. In the present study, although the expression of RIPK1,
255 RIPK3 and MLKL was up-regulated in prostate cancer cells, the possible necroptotic mechanism
256 induced by 20(S)-ginsenoside Rg3 still needs further exploration.
257 The relationship between ROS and necroptosis has been widely explored and abundant evidences
258 confirm they are positively correlated [25, 26]. Early research indicated that RIPK3 could activate
259 several metabolic enzymes which induced aerobic respiration and oxidative respiration, resulting in
260 an increase in ROS production [27]. RIPK1 has been reported to inhibit the activity of the
261 mitochondrial adenine-nucleotide translocase (ANT), which led to a decrease in ADP/ATP
262 exchange and ROS production [28]. Besides, many studies revealed the promoting role of ROS in
263 necroptosis. Previous research reported that ROS mediated the modification of RIPK1 cysteine
264 residues, which facilitated RIPK1 autophosphorylation and subsequent necrosome formation [29].
265 Shikonin, a necroptosis inducer, promoted the overproduction of ROS in nasopharyngeal carcinoma
266 cells and glioma cells, which led to the upregulation of RIPK1 and RIPK3 expression, as well as the
267 induction of necroptosis [30, 31]. A recent study reported that the combined treatment between
268 resveratrol and docetaxel induced apoptosis and necroptosis in prostate cancer cells via ROS
269 production [32]. Another antiproliferative natural compound, curcumin, also induced prostate
270 cancer cell apoptosis and necroptosis, and the reduction of ROS levels could reverse the effects
271 induced by curcumin [33]. Our study also showed that 20(S)-ginsenoside Rg3 upregulated ROS
272 levels in prostate cancer cells, and scavenging ROS with NAC pretreatment antagonized 20(S)-
273 ginsenoside Rg3-induced necroptotic protein expression.
274 The crosstalk between ROS and cell autophagy was well reviewed in a recent report [34]. ROS
275 could transcriptionally and post-transcriptionally regulate cell autophagy, and in turn, autophagy
276 also regulated ROS levels through several pathways. In our study, 20(S)-ginsenoside Rg3-elevated
277 ROS levels induced changes in the autophagy flux in prostate cancer cells. Autophagy also plays an
278 important role in the regulation of necroptosis [35]. An impaired autophagy flux contributed to the
279 induction of necroptosis [36]. In the prostate cancer cell line DU145, sorafenib induced the
280 formation of ATG5-deficient autophagosomes and promoted the interaction between p62 and
281 RIPK1, subsequently triggering necroptosis [37]. Artepillin C (ArtC), a cinnamic acid derivative,
282 induced apoptosis in 22RV1 cells. Co-treatment with ArtC and autophagy inhibitors not only
283 exacerbated apoptosis but also induced necroptosis, suggesting that the inhibition of autophagy may
284 help trigger necroptosis in prostate cancer cells [38]. A previous report has indicated that 20(S)-
285 ginsenoside Rg3 could inhibit autophagic flux in the late stages of autophagy and thus sensitized
286 doxorubicin-induced cell death in hepatocellular carcinoma cell [39]. Our results were consistent

with the report and the autophagy flux was also blocked by 20(S)-ginsenoside Rg3 treatment with an increase in LC3 lipidation and p62 expression in prostate cancer cells, suggesting that the upregulation of p62 induced by 20(S)-ginsenoside Rg3 may contribute to the formation of the necrosome. However, the exact mechanism needs to be further explored.

The present study also evaluated the effect of 20(S)-ginsenoside Rg3 in PC3 mice xenografts. Results indicated that the treatment with 20(S)-ginsenoside Rg3 decreased tumor weight and increased necrotic areas in tumor tissues. Furthermore, 20(S)-ginsenoside Rg3 upregulated the expression of RIPK1, RIPK3 and MLKL in xenograft tissues. However, there was no noteworthy differences in tumor size between control and treated mice, which may be due to the short treatment time.

In conclusion, the present study showed that 20(S)-ginsenoside Rg3 induced the expression of necroptotic proteins in prostate cancer cells *in vitro* and *in vivo*. The underlying mechanism involved ROS accumulation and subsequent autophagy flux impairment.

Acknowledgements: This study was supported by the Sino-Swiss Science and Technology Cooperation (SSSTC) program (Grant: EG 03–032015 to LKS and MC); Tianjin University of Traditional Chinese Medicine Foundation (to LKS); National Natural Science Foundation of China (No. 81873100 to SWZ).

References

[1] BRAY F, LAVERSANNE M, SUNG H, FERLAY J, SIEGEL RL et al. Global cancer statistics 2022: GLOBOCAN estimates of incidence and mortality worldwide for 36 cancers in 185 countries. CA Cancer J Clin 2024; 74: 229-263. https://doi.org/10.3322/caac.21834

[2] COHEN MB, ROKHLIN OW. Mechanisms of prostate cancer cell survival after inhibition of AR expression. J Cell Biochem 2009; 106: 363-371. https://doi.org/10.1002/jcb.22022

[3] TONG X, TANG R, XIAO M, XU J, WANG W et al. Targeting cell death pathways for cancer therapy: recent developments in necroptosis, pyroptosis, ferroptosis, and cuproptosis research. J Hematol Oncol 2022; 15: 174. https://doi.org/10.1186/s13045-022-01392-3

[4] BERETTA GL, ZAFFARONI N. Necroptosis and Prostate Cancer: Molecular Mechanisms and Therapeutic Potential. Cells 2022; 11: 1221. https://doi.org/10.3390/cells11071221

[5] MONTAGNANI MARELLI M, BERETTA G, MORETTI RM. Necroptosis Induced by Delta-Tocotrienol Overcomes Docetaxel Chemoresistance in Prostate Cancer Cells. Int J Mol Sci 2023; 24: 4923. https://doi.org/10.3390/ijms24054923

[6] KOO GB, MORGAN MJ, LEE DG, KIM WJ, YOON JH et al. Methylation-dependent loss of RIP3 expression in cancer represses programmed necrosis in response to chemotherapeutics. Cell Res 2015; 25: 707-725. https://doi.org/10.1038/cr.2015.56

[7] HEIDARYAN F, BAMEHR H, BABAABASI B, EMAMVIRDIZADEH A, MOHAMMADZADEH N et al. The Trend of ripk1/ripk3 and mlkl Mediated Necroptosis

Pathway in Patients with Different Stages of Prostate Cancer as Promising Progression Biomarkers. Clin Lab 2020; 66. https://doi.org/10.7754/Clin.Lab.2019.190439

[8] WANG KJ, WANG KY, ZHANG HZ, MENG XY, CHEN JF et al. Up-Regulation of RIP3 Alleviates Prostate Cancer Progression by Activation of RIP3/MLKL Signaling Pathway and Induction of Necroptosis. Front Oncol 2020; 10: 1720. https://doi.org/10.3389/fonc.2020.01720

[9] FU W, LI H, FU H, ZHAO S, SHI W et al. The SIRT3 and SIRT6 Promote Prostate Cancer Progression by Inhibiting Necroptosis-Mediated Innate Immune Response. J Immunol Res 2020; 2020: 8820355. https://doi.org/10.1155/2020/8820355

[10] LU Z, WU C, ZHU M, SONG W, WANG H et al. Ophiopogonin D' induces RIPK1dependent necroptosis in androgendependent LNCaP prostate cancer cells. Int J Oncol 2020; 56: 439-447. https://doi.org/10.3892/ijo.2019.4945

[11] LEE YJ, NAM HS, CHO MK, LEE SH. Arctigenin induces necroptosis through mitochondrial dysfunction with CCN1 upregulation in prostate cancer cells under lactic acidosis. Mol Cell Biochem 2020; 467: 45-56. https://doi.org/10.1007/s11010-020-03699-6

[12] XU H, ZENG X, WEI X, XUE Z, CHEN N et al. Rosin Derivative IDOAMP Inhibits Prostate Cancer Growth via Activating RIPK1/RIPK3/MLKL Signaling Pathway. Oxid Med Cell Longev 2022; 2022: 9325973. https://doi.org/10.1155/2022/9325973

[13] ZHOU X, YEASMIN KHUSBU F, XIE Y, YANG P. Emodin-Induced Necroptosis in Prostate Cancer Cells via the Mitochondrial Fission HSP90/MLKL/PGAM Pathway. Chem Biodivers 2023; 20: e202201130. https://doi.org/10.1002/cbdv.202201130

[14] GAO S, FANG C, WANG T, LU W, WANG N et al. The effect of ginsenoside Rg3 combined with chemotherapy on immune function in non-small cell lung cancer: A systematic review and meta-analysis of randomized controlled trials. Medicine (Baltimore) 2023; 102: e33463. https://doi.org/10.1097/MD.0000000000033463

[15] NAKHJAVANI M, SMITH E, YEO K, TOMITA Y, PRICE TJ et al. Differential antiangiogenic and anticancer activities of the active metabolites of ginsenoside Rg3. J Ginseng Res 2024; 48: 171-180. https://doi.org/10.1016/j.jgr.2021.05.008

[16] KIM HS, LEE EH, KO SR, CHOI KJ, PARK JH et al. Effects of ginsenosides Rg3 and Rh2 on the proliferation of prostate cancer cells. Arch Pharm Res 2004; 27: 429-435. https://doi.org/10.1007/BF02980085

[17] KIM SM, LEE SY, CHO JS, SON SM, CHOI SS et al. Combination of ginsenoside Rg3 with docetaxel enhances the susceptibility of prostate cancer cells via inhibition of NF-kappaB. Eur J Pharmacol 2010; 631: 1-9. https://doi.org/10.1016/j.ejphar.2009.12.018

[18] PAN XY, GUO H, HAN J, HAO F, AN Y et al. Ginsenoside Rg3 attenuates cell migration via inhibition of aquaporin 1 expression in PC-3M prostate cancer cells. Eur J Pharmacol 2012; 683: 27-34. https://doi.org/10.1016/j.ejphar.2012.02.040

[19] PENG Y, ZHANG R, YANG X, ZHANG Z, KANG N et al. Ginsenoside Rg3 suppresses the proliferation of prostate cancer cell line PC3 through ROS-induced cell cycle arrest. Oncol Lett 2019; 17: 1139-1145. https://doi.org/10.3892/ol.2018.9691

[20] PENG Y, ZHANG R, KONG L, SHEN Y, XU D et al. Ginsenoside Rg3 inhibits the senescence of prostate stromal cells through down-regulation of interleukin 8 expression. Oncotarget 2017; 8: 64779-64792. https://doi.org/10.18632/oncotarget.17616

[21] DAI W, CHENG J, LENG X, HU X, AO Y. The potential role of necroptosis in clinical diseases (Review). Int J Mol Med 2021; 47: 89. https://doi.org/10.3892/ijmm.2021.4922

[22] GENG J, ITO Y, SHI L, AMIN P, CHU J et al. Regulation of RIPK1 activation by TAK1-mediated phosphorylation dictates apoptosis and necroptosis. Nat Commun 2017; 8: 359. https://doi.org/10.1038/s41467-017-00406-w

[23] WANG L, CHANG X, FENG J, YU J, CHEN G. TRADD Mediates RIPK1-Independent Necroptosis Induced by Tumor Necrosis Factor. Front Cell Dev Biol 2019; 7: 393. https://doi.org/10.3389/fcell.2019.00393

[24] WEINELT N, WACHTERSHAUSER KN, CELIK G, JEILER B, GOLLIN I et al. LUBAC-mediated M1 Ub regulates necroptosis by segregating the cellular distribution of active MLKL. Cell Death Dis 2024; 15: 77. https://doi.org/10.1038/s41419-024-06447-6

[25] HSU SK, CHANG WT, LIN IL, CHEN YF, PADALWAR NB et al. The Role of Necroptosis in ROS-Mediated Cancer Therapies and Its Promising Applications. Cancers (Basel) 2020; 12: 2185. https://doi.org/10.3390/cancers12082185

[26] CAI H, MENG Z, YU F. The involvement of ROS-regulated programmed cell death in hepatocellular carcinoma. Crit Rev Oncol Hematol 2024; 197: 104361. https://doi.org/10.1016/j.critrevonc.2024.104361

[27] ZHANG DW, SHAO J, LIN J, ZHANG N, LU BJ et al. RIP3, an energy metabolism regulator that switches TNF-induced cell death from apoptosis to necrosis. Science 2009; 325: 332-336. https://doi.org/10.1126/science.1172308

[28] TEMKIN V, HUANG Q, LIU H, OSADA H, POPE RM. Inhibition of ADP/ATP exchange in receptor-interacting protein-mediated necrosis. Mol Cell Biol 2006; 26: 2215-2225. https://doi.org/10.1128/MCB.26.6.2215-2225.2006

[29] ZHANG Y, SU SS, ZHAO S, YANG Z, ZHONG CQ et al. RIP1 autophosphorylation is promoted by mitochondrial ROS and is essential for RIP3 recruitment into necrosome. Nat Commun 2017; 8: 14329. https://doi.org/10.1038/ncomms14329

[30] LU B, GONG X, WANG ZQ, DING Y, WANG C et al. Shikonin induces glioma cell necroptosis in vitro by ROS overproduction and promoting RIP1/RIP3 necrosome formation. Acta Pharmacol Sin 2017; 38: 1543-1553. https://doi.org/10.1038/aps.2017.112

[31] LIU T, SUN X, CAO Z. Shikonin-induced necroptosis in nasopharyngeal carcinoma cells via ROS overproduction and upregulation of RIPK1/RIPK3/MLKL expression. Onco Targets Ther 2019; 12: 2605-2614. https://doi.org/10.2147/OTT.S200740

[32] LEE SH, LEE YJ. Synergistic anticancer activity of resveratrol in combination with docetaxel in prostate carcinoma cells. Nutr Res Pract 2021; 15: 12-25. https://doi.org/10.4162/nrp.2021.15.1.12

[33] LEE YJ, PARK KS, LEE SH. Curcumin Targets Both Apoptosis and Necroptosis in Acidity-Tolerant Prostate Carcinoma Cells. Biomed Res Int 2021; 2021: 8859181. https://doi.org/10.1155/2021/8859181

[34] DONG L, HE J, LUO L, WANG K. Targeting the Interplay of Autophagy and ROS for Cancer Therapy: An Updated Overview on Phytochemicals. Pharmaceuticals (Basel) 2023; 16: 92. https://doi.org/10.3390/ph16010092

[35] ZHANG L, CUI T, WANG X. The Interplay Between Autophagy and Regulated Necrosis. Antioxid Redox Signal 2023; 38: 550-580. https://doi.org/10.1089/ars.2022.0110

[36] ZHANG H, YIN Y, LIU Y, ZOU G, HUANG H et al. Necroptosis mediated by impaired autophagy flux contributes to adverse ventricular remodeling after myocardial infarction. Biochem Pharmacol 2020; 175: 113915. https://doi.org/10.1016/j.bcp.2020.113915

[37] KHARAZIHA P, CHIOUREAS D, BALTATZIS G, FONSECA P, RODRIGUEZ P et al. Sorafenib-induced defective autophagy promotes cell death by necroptosis. Oncotarget 2015; 6: 37066-37082. https://doi.org/10.18632/oncotarget.5797

[38] ENDO S, HOSHI M, MATSUNAGA T, INOUE T, ICHIHARA K et al. Autophagy inhibition enhances anticancer efficacy of artepillin C, a cinnamic acid derivative in Brazilian green propolis. Biochem Biophys Res Commun 2018; 497: 437-443. https://doi.org/10.1016/j.bbrc.2018.02.105

[39] KIM DG, JUNG KH, LEE DG, YOON JH, CHOI KS et al. 20(S)-Ginsenoside Rg3 is a novel inhibitor of autophagy and sensitizes hepatocellular carcinoma to doxorubicin. Oncotarget 2014; 5: 4438-4451. https://doi.org/10.18632/oncotarget.2034

Figure Legends

Figure 1. Analysis of necroptotic gene expression based on GTEx and TCGA databases. A) Expression of *RIPK1, RIPK3* and *MLKL* in normal prostate and prostate tumor tissues. B) Expression of *RIPK1*, *RIPK3* and *MLKL* in prostate tumor tissues and corresponding para-cancerous tissues. C) ROC analysis of the diagnostic efficiency of the three genes in prostate cancer. D) Disease specific survival analysis of *RIPK3* expression in prostate cancer. PRAD, prostate adenocarcinoma. *$p < 0.05$, ***$p < 0.001$ vs. Normal

Figure 2. 20(S)-ginsenoside Rg3 inhibited cell proliferation and increased the proportion of necroptotic cells in prostate cancer cells. A) CCK8 assays to evaluate the effects of 20(S)-ginsenoside Rg3 on the proliferation of 22RV1 cells. B) CCK8 assays to evaluate the effects of 20(S)-ginsenoside Rg3 on the proliferation of PC3 cells. C) Flow cytometry analysis of apoptotic and necrotic cells in prostate cancer cells treated with DMSO or 100 μM 20(S)-ginsenoside Rg3 for 48 h. D, E) Quantitative analysis of flow cytometry results. F) Western blot assays for the expression and cleavage of caspase 3 in 22RV1 and PC3 cells treated with 100 μM 20(S)-ginsenoside Rg3 for 48 h. *$p < 0.05$, **$p < 0.01$ vs. CTRL

Figure 3. 20(S)-ginsenoside Rg3 up-regulated the expression of necroptotic proteins in prostate cancer cells. A) Western blot assays for the expression of necroptotic proteins in 22RV1 and PC3 cells treated with 100 μM 20(S)-ginsenoside Rg3 for 48 h. B) Quantitative analysis of protein expression in 22RV1 and PC3 cells. C) CCK8 assays to explore the proliferation of 22RV1 and PC3 cells pretreated with 100 μM Nec-1 for 1 h. *$P<0.05$, **$P<0.01$ vs CTRL

Figure 4. 20(S)-ginsenoside Rg3 blocked autophagy flux and up-regulated the expression of necroptotic proteins in prostate cancer cells via overproduction of ROS. A) Flowcytometry analysis of ROS levels in 22RV1 and PC3 cells treated with 100 μM 20(S)-ginsenoside Rg3 for 48 h. B) Western blot showing LC3 lipidation and p62 expression in 22RV1 and PC3 cells treated with 50 or 100 μM 20(S)-ginsenoside Rg3 for 48 h. C) Quantitative analysis of the lipidation of LC3 and the expression of p62 in 22RV1 and PC3 cells treated with different doses of 20(S)-ginsenoside Rg3. D) Western blotting showing the effects of 100 μM 20(S)-ginsenoside Rg3 on LC3 lipidation and p62

expression in 22RV1 and PC3 cells pretreated with 10 mM NAC for 1 h. E) Quantitative analysis of LC3 lipidation and p62 expression in 22RV1 and PC3 cells. F) Western blotting showing the effects of 100 μM 20(S)-ginsenoside Rg3 on the expression of necroptotic proteins in 22RV1 and PC3 cells pretreated with 10 mM NAC for 1 h. G) Quantitative analysis of necroptotic proteins expression in 22RV1 and PC3 cells. C, CTRL; R, 20(S)-ginsenoside Rg3; N, NAC; N+R, NAC+20(S)-ginsenoside Rg3. *$p < 0.05$, **$p < 0.01$ vs. CTRL

Figure 5. 20(S)-ginsenoside Rg3 up-regulated necroptotic protein expression in a PC3 mouse xenograft model. A) Xenografts isolated from control mice and 20(S)-ginsenoside Rg3-treated mice. B) tumor volume in both control and ginsenoside Rg3-treated mice. C) Tumor weights from control and 20(S)-ginsenoside Rg3-treated mice. D) HE staining of tumor tissues isolated from control and 20(S)-ginsenoside Rg3-treated mice. E) IF staining analysis of the expression of RIPK1, RIPK3 and MLKL in xenograft tissues. F) Protein expression of RIPK1, RIPK3 and MLKL in tumor tissues. G) Quantitation analysis of the results of western blot. *$p < 0.05$, **$p < 0.01$ vs. CTRL

Fig. 1 Download full resolution image

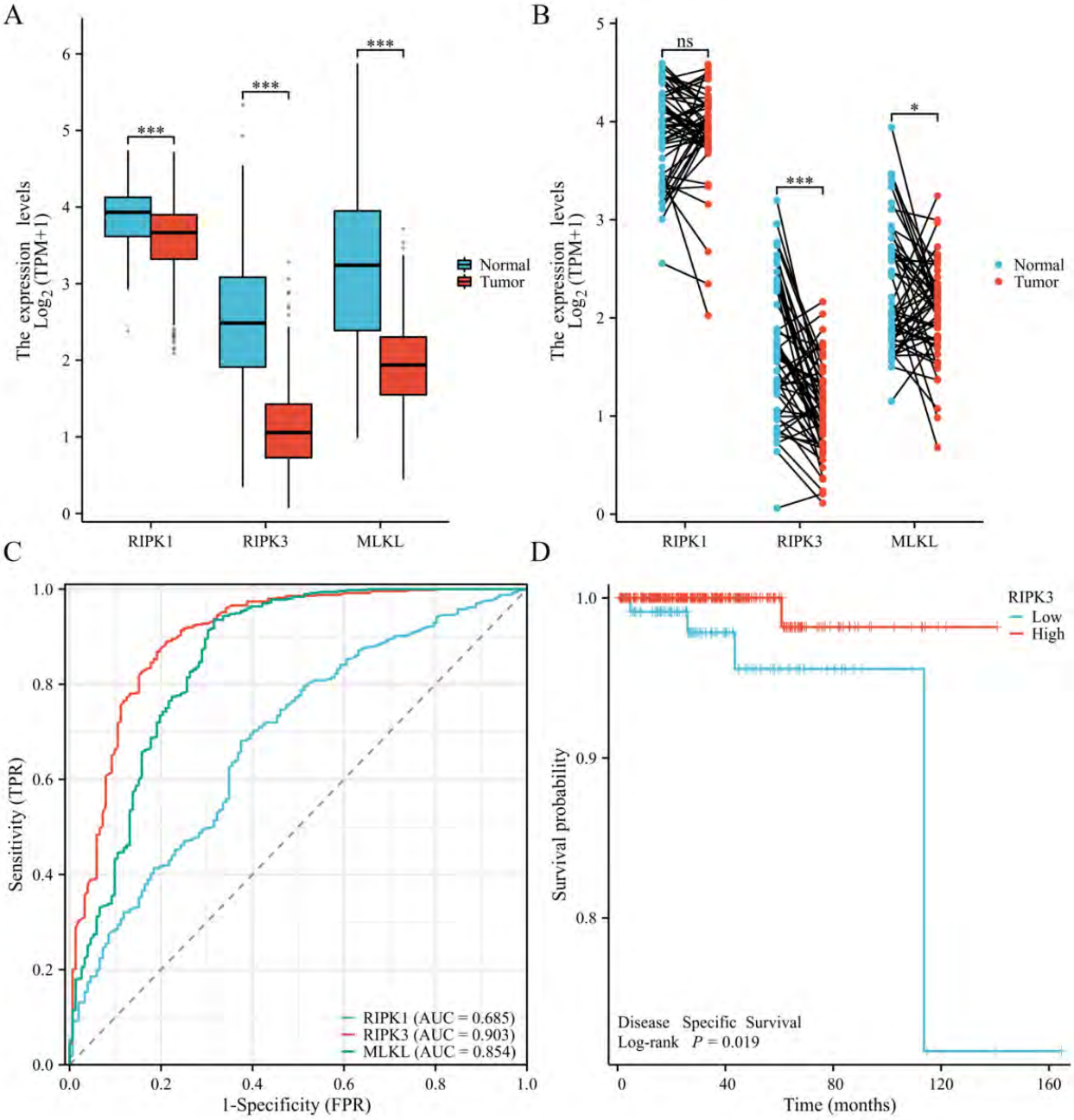

Fig. 2 Download full resolution image

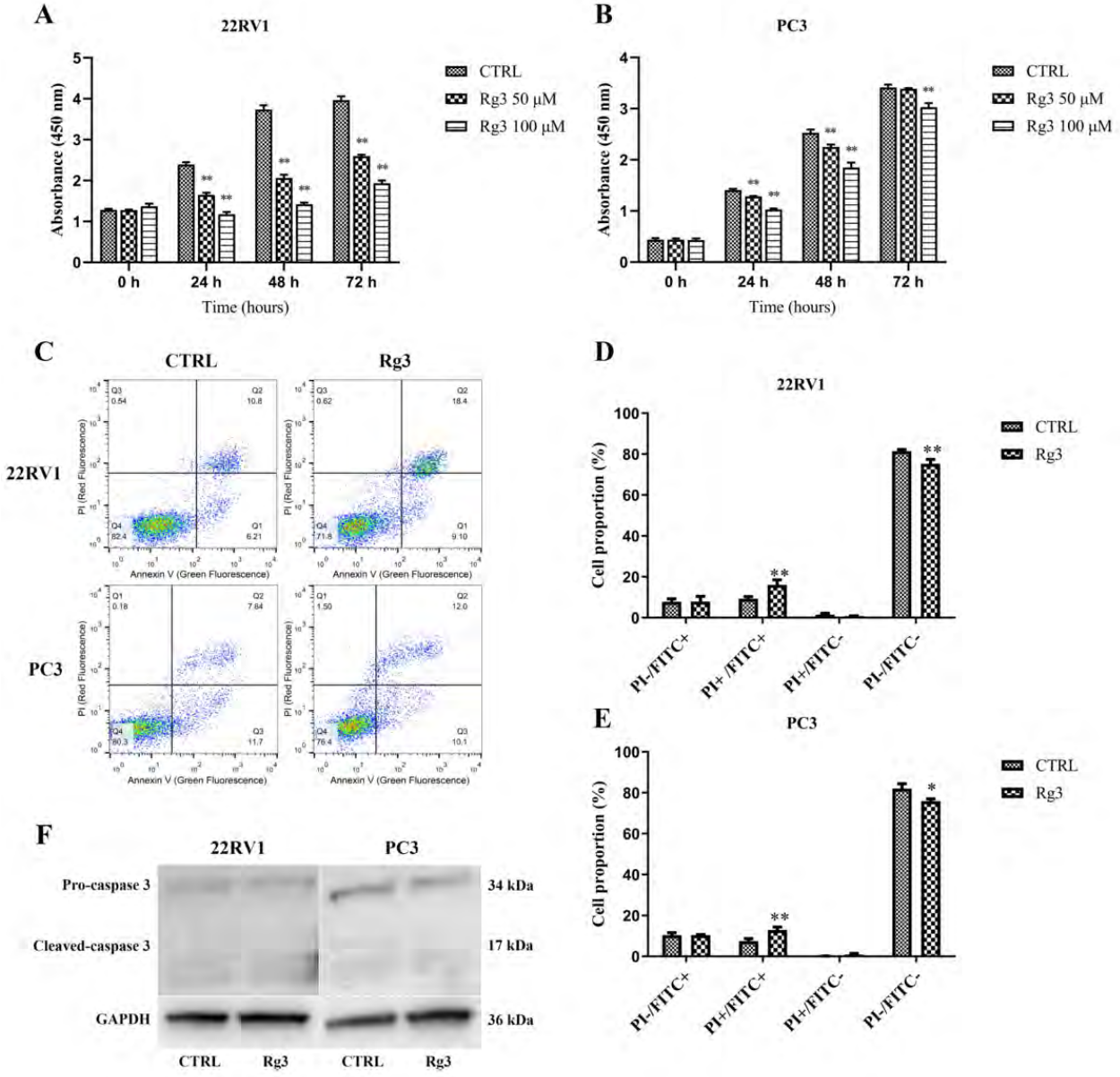

Fig. 3 Download full resolution image

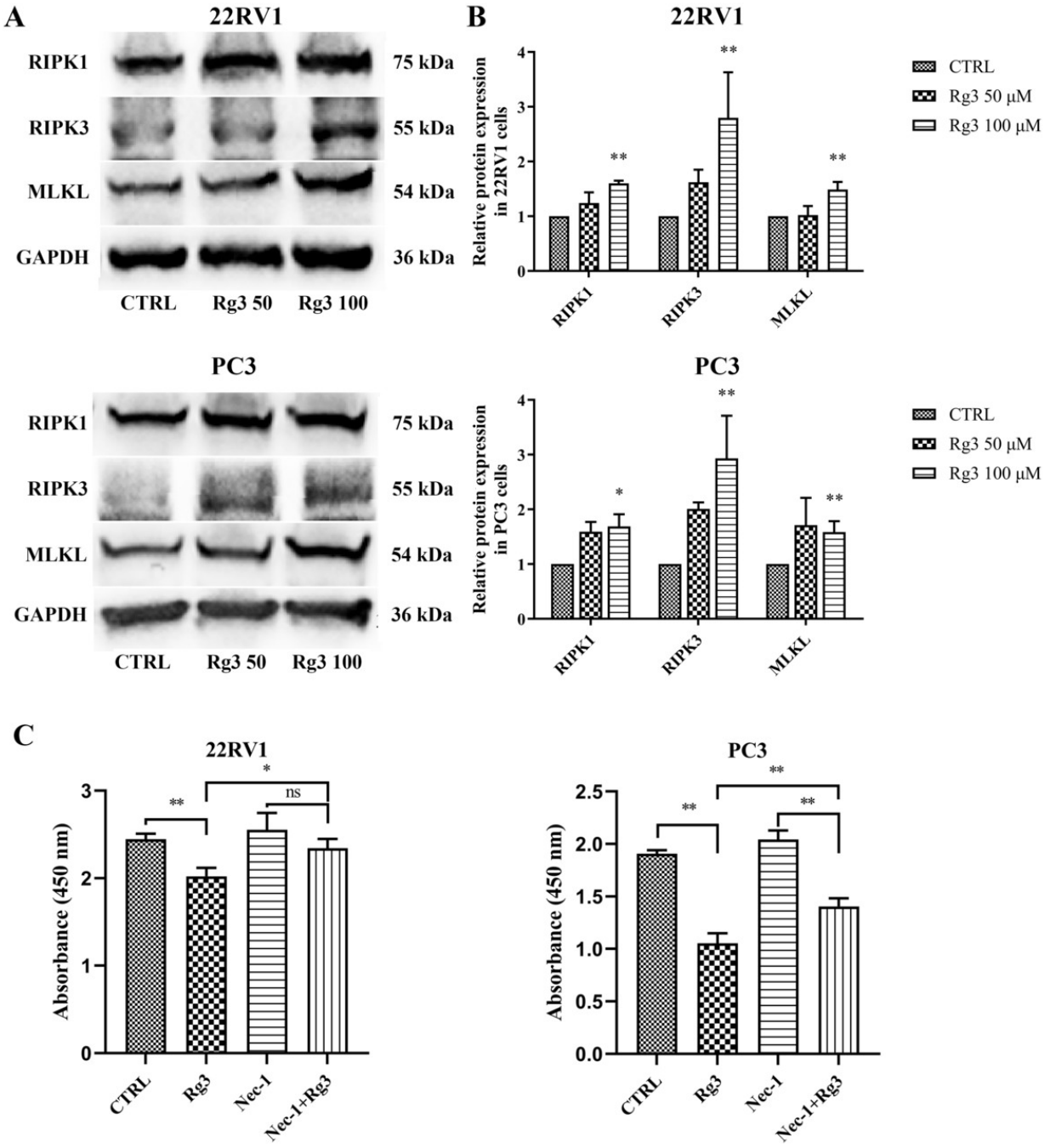

Fig. 4 Download full resolution image

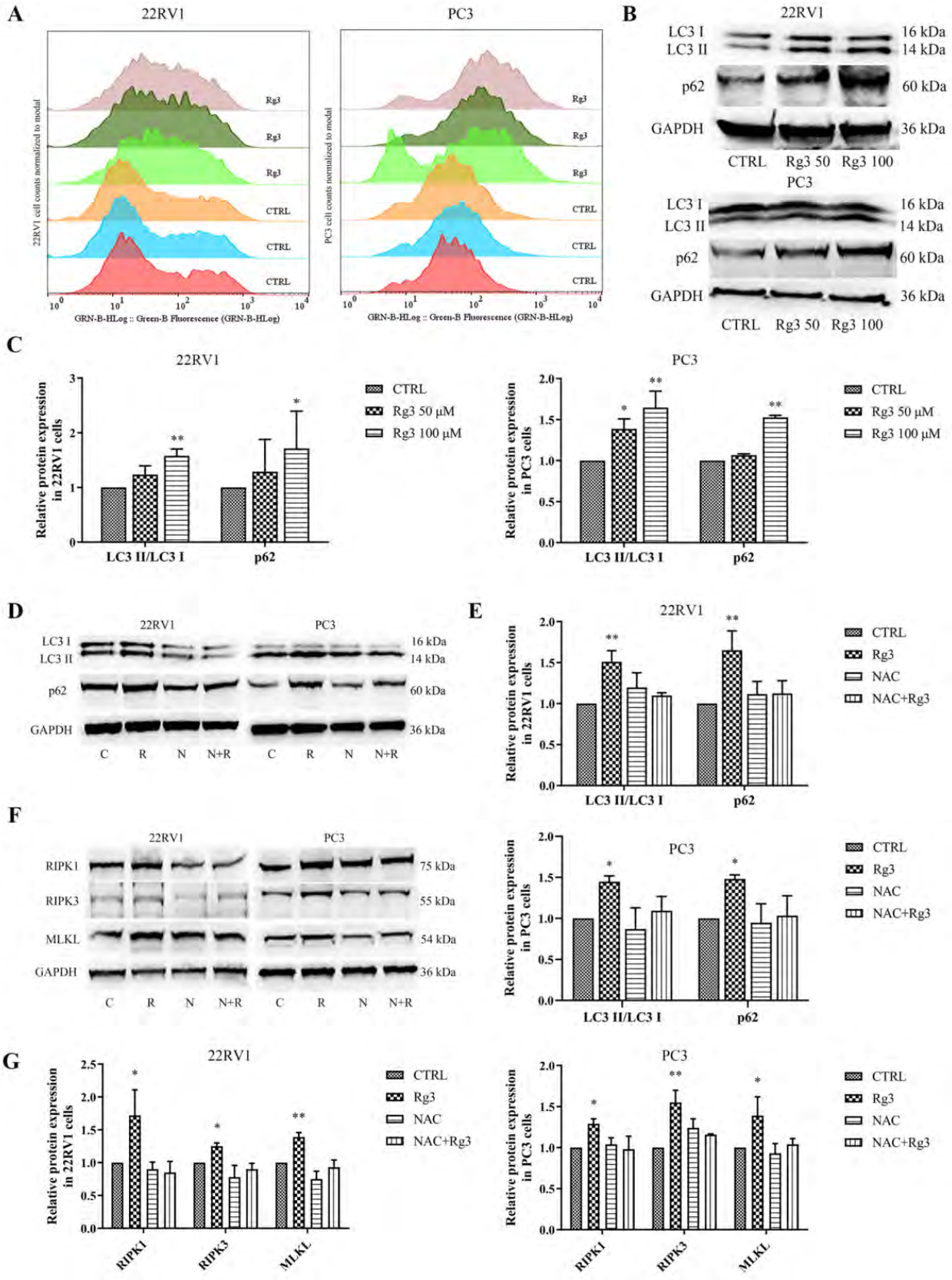

Fig. 5 Download full resolution image